Heritage Science

RESEARCH

Open Access

The quantification of physico-mechanical properties and durability of onyx-travertines from Santa Ana de los Ríos de Cuenca, Ecuador

Martha Romero Bastidas[1], María del Cisne Aguirre Ullauri[2,3*], Johanna Ramírez Bustamante[1], Michel Vargas Vallejo[4] and Edison Castillo Carchipulla[2]

Abstract

In this study, physico-mechanical properties and durability of 4 onyx-travertines from Sinincay (Ecuador) were investigated. These onyx-travertines are commonly used for decorative purposes in buildings in the Historic Center of Santa Ana de los Ríos de Cuenca. The aim of this work was to characterize these stones and determine the variation of their physico-mechanical properties, such as mass loss and water absorption, after being subjected to four durability tests: salt crystallization (S-C), freeze–thaw (F-T), thermal shock (T-S) and acid attack (A-A). In addition, Scanning Electron Microscopic (SEM) analyses were carried out to record weathering patterns and understand the deterioration mechanism. Results show that these stones' sedimentary structure is stratified. Two specimens exhibit geometrical features consistent with porous laminated facies and the remaining two have slightly porous cryptolaminated ones. Facies' structure orientation is also found to determine mechanical strength, exhibiting the normal to lamination orientation the lowest value. As for durability, the statistical interpretation of the results suggests that the level of severity of each test follows S-C > F–T > A-A > T-S. In addition, laminated facies are more vulnerable to accelerated aging tests. Impact of S-C, F–T and T-S tests is mainly explained by differences in porosity and damage produced by A-A is related to the available effective area for the reaction to take place. Thus, the onyx-travertine is more than a wonderful material, it represents an interesting case study for development of future research on heritage stone in Ecuador and the world by employing normalized tests that are rarely used or published.

Keywords: Onyx-travertine, Porosity, Accelerated aging, Capillarity, Salt crystallization, Freezing–thawing, Thermal shock, Acid attack

Introduction

As a natural material, the term travertine refers to the sedimentary stones produced by intense underwater pressure in the presence of carbonate-rich solutions that come from various depositional environments of sedimentary basins [1, 2]. This condition explains changes in the chemical, physical, mechanical and petrographic properties of the stone [3, 4]. For example, Akyol et al. [3] divided Denizli travertines into four lithotypes including shrub, crystalline crust (onyx), reed, and noche.

Onyx- travertine is commonly formed as a result of the pressure achieved due to fast flowing water on a gentle slope. Some onyx-travertines consist of the alternation of white, red and brown colored layers (the latter two due to high iron content in the hot water springs) [5]. They also show dense, crudely fibrous and light-colored layers that are composed of elongated calcite feathers developed perpendicular to the deposit surface [6]. Onyx-travertine deposits are strongly linked to the presence of ancient volcanic activity. Ecuador is one of the countries of origin of the majority of the onyx traded today [7].

*Correspondence: maguirreu@ucacue.edu.ec

[2] Universidad Politécnica de Madrid/Polytechnic University of Madrid, Madrid, Spain

Full list of author information is available at the end of the article

Onyx-travertine is one of the natural stones that has been successfully used in the Historic Center of Santa Ana de los Rios de Cuenca. It has been used for visual effect due to its translucency when polished. The main architectural style associated with its use is Neoclassical [8, 9]. The city's urban-architectural image is determined by the presence of onyx-travertines in a wide variety of colors within walls, sidewalks and squares [10]. Pink onyx-travertine predominates, as seen in Fig. 1. According to historical sources, these rocks come from quarries in the area of Pumayunga, Sinincay [11–13] and other places on the outskirts of the city.

The degradation of a stone is a natural and irreversible process. As a result, any building constructed with stone is prone to decay, more or less; rapidly, depending on its intrinsic properties and the surrounding environment. According to several authors [14–20], the main causes of deterioration of travertine are the crystallization/hydration of salts, and the freezing–thawing and acidic environments, with the crystallization of salts being the most harmful agent of deterioration.

Salt crystallization (S-C) occurs when saline solutions infiltrate through the pores of the stone and soluble salts precipitate due to changes in humidity and temperature [21, 22]. Soluble salts in buildings mainly originate from: a) ions leached due the deterioration of rocks, mortars, bricks and other building materials, b) soil, c) deposition of atmospheric products and d) biogenerated, in which the most important sources are human and animal urine [23]. Freezing–thawing (F–T) is generally caused by temperatures fluctuating below and above 0 °C in stones containing a certain amount of water [24]. The harmful effect of S-C and F–T of water inside the pores or cracks within the stones, results from the pressure exerted by the salt crystals and ice when their size increases, generating an internal pressure that exceeds the strength of the stone [25, 26].

On the other hand, acidic environments also affect the durability of travertines due to their carbonated nature [27]. Previous studies of Iranian onyx-travertines have shown that this stone type has a lower effective porosity and higher mechanical properties, such as Brazilian Tensile Strength (BTS), Point Load Strength Index (PLSI) and P-wave Velocity, in comparison to other lithotypes. These studies also reveal that onyx-travertines offer greater durability, since they present greater resistance to the salt crystallization pressure, having higher effective porosity and mechanical properties [28]. Alveolar and granular disintegration due to salt crystallization pressure were also observed, but there was no significant loss of integrity [29, 30].

All of them have in common that they are selective, accelerated and practical tests; however, there is still no commonly accepted test protocol, owing to both the limitations of current standard methods and the different study objectives. At present, there are several standards and recommendations (RILEM, UNE-EN, ASTM, DIN, CNR…) that do not always take into account all the variables that affect the test and do not provide criteria for the evaluation and classification of the durability of the tested material. Thus, in these publications, the conclusions are obtained only by comparison between the different materials tested (relative classification) [31, 32].

The present study is attempt to characterize the physical–mechanical properties and durability of Sinincay onyx-travertine, with special emphasis on the influence of both mechanical and chemical weathering agents, including the crystallization of soluble salts, frost action, thermal shock and acid solutions on the quality of these stones, using internationally established methods, to facilitate comparative analysis with other similar studies. This knowledge is not only useful for proposing preventive architectural conservation measures based on the prediction of their behavior over time, but also for the selection of the appropriate onyx-travertine to be used as building and/or replacement stone in architectural restoration not only in the Historic Center of Cuenca in Ecuador, but also in other parts of the world.

Materials and methods

Materials

The four types of onyx-travertines typically found in local heritage buildings (Fig. 1) were obtained from the quarry of Sinincay, Pumayunga, located in coordinates 71° 94′ 41.88″; 96° 82′ 07.04″. Specimens were identified and labeled as follows: (1) PT (pink onyx-travertine), (2) YT (yellow onyx- travertine), (3) WT (white onyx-travertine), and (4) GT (gray onyx-travertine). The characterization and durability tests were performed in two orientations, normal and parallel to the lamination. Figure 2 shows the samples.

The careful selection of samples for obtaining test specimens was performed based on visual comparison of perceptible color and texture with typical onyx-travertine found in buildings of the Historic Center of Cuenca.

Methods

Figure 3 shows the methodological approach followed in this work for the physico-chemical characterization and durability assessment of these travertines. All petrographic, chemical and physico-mechanical properties and durability tests were carried out in the Laboratory and Analysis Unit of the National Institute of Cultural Heritage of Ecuador, except compression and flexural tests, which were performed in the Geotechnical and

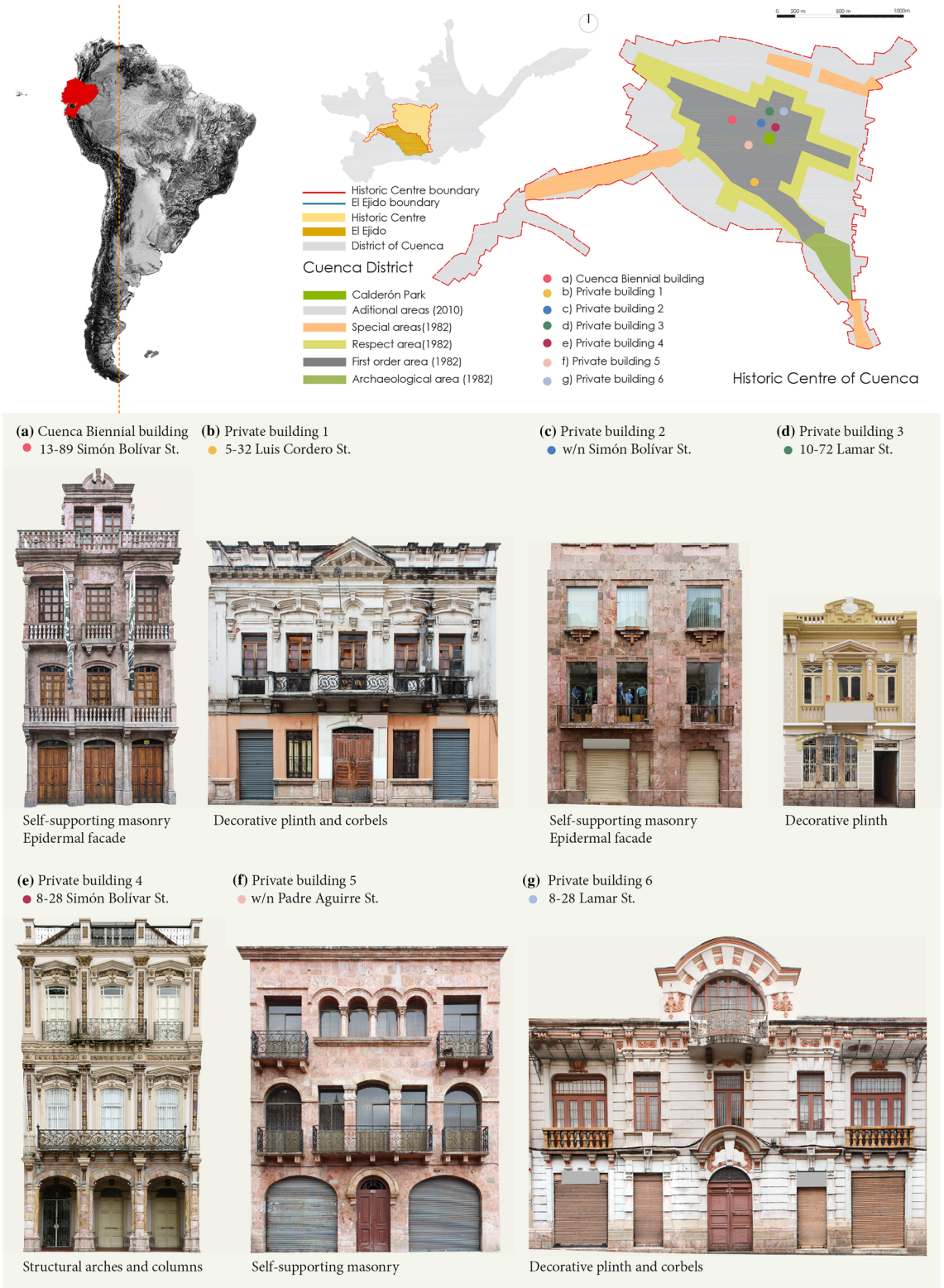

Fig. 1 Use of onyx-travertines in the Historic Center of Cuenca

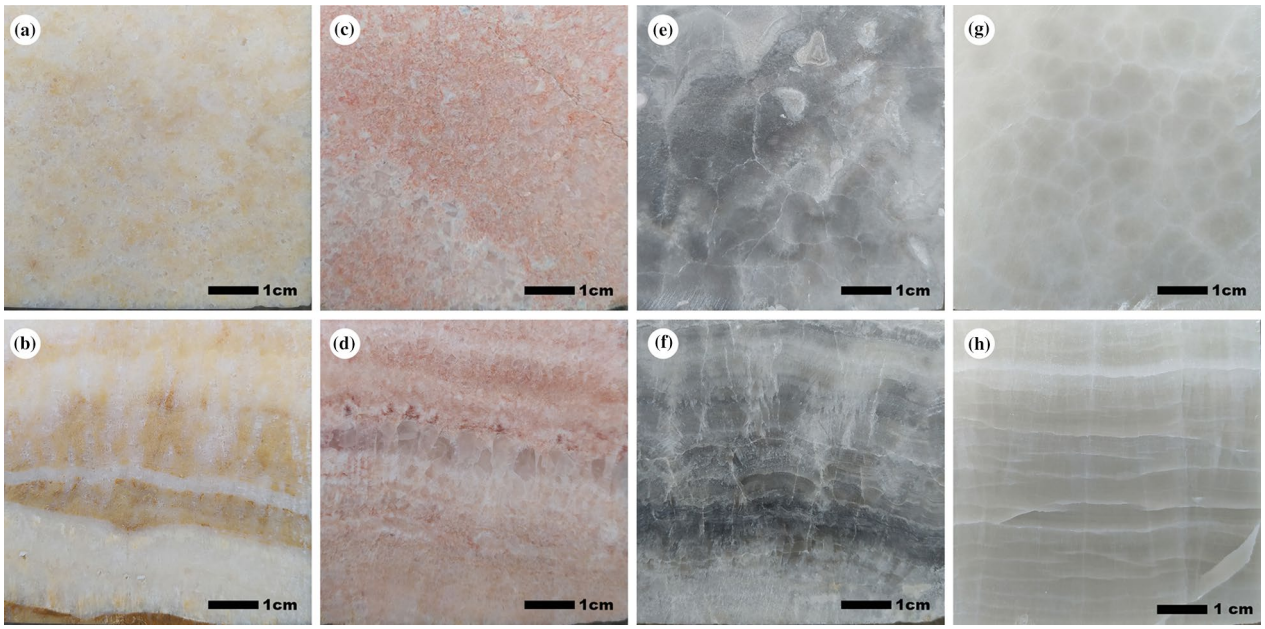

Fig. 2 According to the lamination, onyx-travertine appearance has two main variations: parallel and normal to lamination. Photographs of typical observed surfaces of test specimens are presented: YT (**a**, **b**), PT (**c**, **d**), GT (**e**, **f**), WT (**g**, **h**). Parallel to the lamination: **a**, **c**, **e**, **g**; Normal to the lamination: **b**, **d**, **f**, **h**

Materials Laboratory of the Faculty of Engineering at the University of Cuenca.

Chemical and mineralogical composition

Chemical composition was determined by X-Ray Energy Dispersive Spectroscopy (EDS) using an Oxford X-MAX 20 detector in a variable pressure scanning electron microscope (Jeol IT300), at low pressure (40 Pa), acceleration voltage of 20 kV, probe current of 25 mA and working distance of 10 mm.

The mineralogical composition was determined by using an X-ray Diffractometer (XRD) (Bruker Advance D8). The powder method was used. Samples were crushed in an agate mortar and pestle, then sieved in a #240 mesh grit. Analytical conditions were: voltage of 35 kV, current of 35 mA, step of 0.6 s, 2Θ from 5° to 72° with increments of 0.021°. Software used for identification and quantification of the crystalline phases was TOPAS, version 4.2.

Petrographic characterization

Thin sections of samples were prepared in two cuts, normal and parallel to lamination for each type of travertine using a diamond saw. Samples were then adhered to a glass slide using Entellan™ resin and sanded with silicon carbide paper (#400, #1000, #1200 and #1500 grit size), and polished using tungsten carbide dispersion powder of 150 microns. Specimens were then examined using a polarized light microscope (Nikon Eclipse e200) and a phase contrast microscope (Zeiss Axioscope A1). The microscopic study was complemented by examining samples in a variable pressure scanning electron microscope (Jeol IT300) using a back-scattered electron detector at low pressure (between 30 and 50 Pa), probe current of 25 mA, acceleration voltages between 20 and 25 kV, and working distance of 10 mm. Observations were focused on the analysis of sedimentary structures and morphological features. Classification was made according to the structure and content of the micritic matrix [31]. Finally, a detailed study of pore structure and shape in the polished sections stained with methylene blue was carried out using an optical microscope with phase contrast (Zeiss Scope A1). The classification of Choquette and Pray [34] was used, which includes: the basic type of porosity, the formation time and the size and volume of pores in reference to the total volume of the stone.

Petrophysical properties

The petrophysical properties were studied using water immersion test methods. Consequently, pore size distribution and pore shape could not be reported. For open porosity, which represents the volume of pores that show a certain degree of interconnection with the exterior faces of the sample, the direct measurement was made in 3 cubic specimens by size $70 \times 70 \times 70$ mm of each type of travertine. Water saturation of specimens

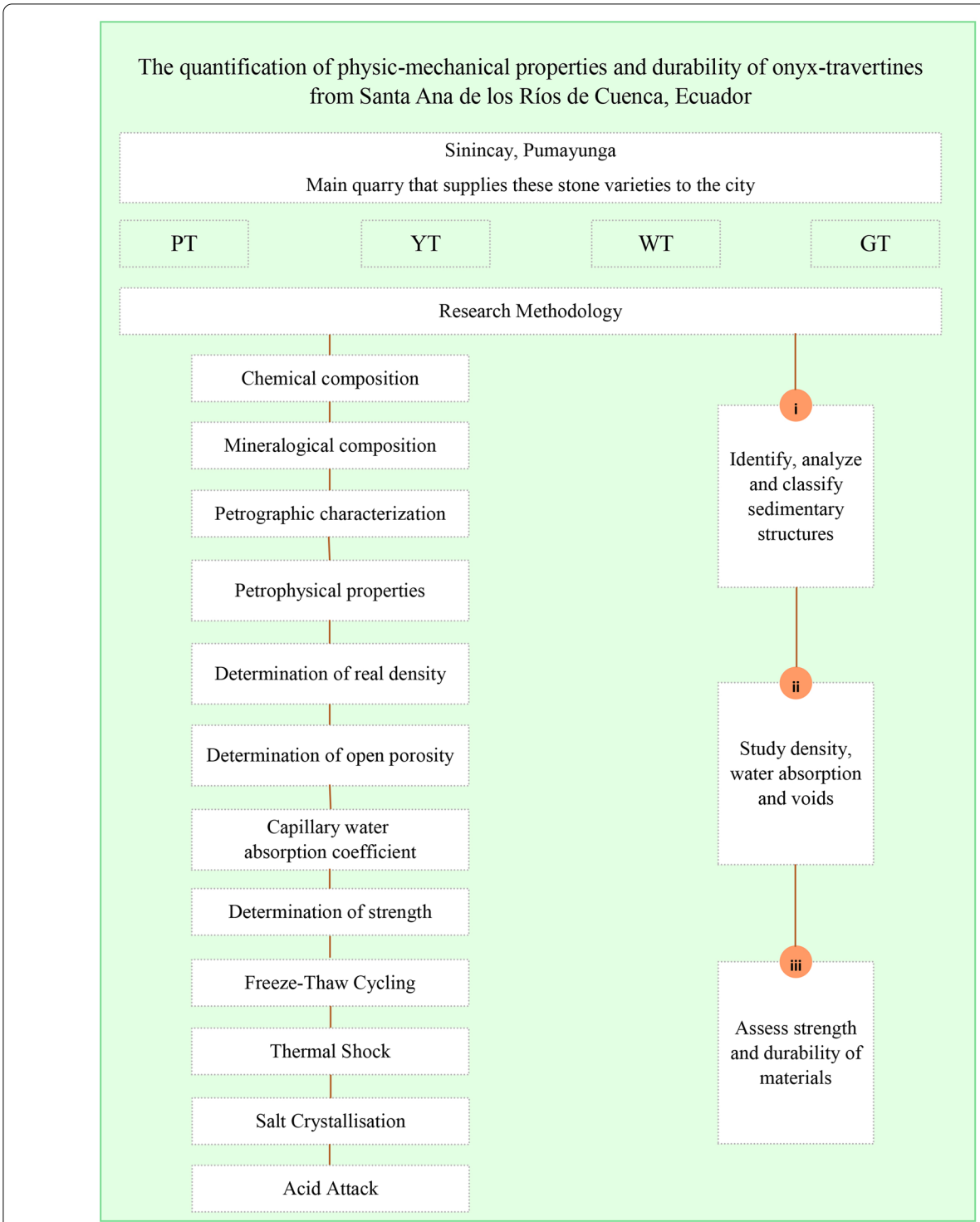

Fig. 3 Methodology used in this research

was carried out by immersion until a constant mass was obtained, given by the difference between two successive weighings not greater than 0.1%. Determination of real density and open porosity was achieved based on the Spanish standard test method UNE-EN 1936 [35]. Real density excludes porosity and is calculated from the ratio between the mass of the dry rock and the volume of the solid fraction; for which the water pycnometer method

was employed using pulverized samples with a particle size of less than 0.063 mm.

Water absorption by capillarity was determined using the standard test method UNE EN-1925 [36]. Three cubic specimens sized 70 × 70 × 70 mm of each type of travertine were used, which, once dry, are submerged from the base until reaching a depth of 3 mm. The time is registered and the depth is kept constant until the end of the test.

Mechanical properties

Strength was the only mechanical property evaluated in this work by performing compression and flexural tests. Standard test methods of UNE-EN 1926 [37] and ASTM 99–87 [38] (equivalent to UNE-EN 12372: 2007) were followed using a hydraulic universal press (Shimadzu Concrete 2000X press). Test conditions were 1 MPa/s applied in the compression test and 0.6 MPa/s in the 3-point bending test [37, 38]. Six specimens were tested for each type of travertine, although the specified number of specimens in the standard procedure in each cut direction according to its anisotropic plane is higher. This number was modified due to commonly reported high variations in stone strength values as a result of variations in internal structure, material cost, and technical limitations for cutting, leveling, sanding and polishing. The specimen dimensions were 10 cm × 20 cm × 6 cm.

Ozkul et al. [39] the unconfined compressive strength of travertine varies according to the test directions and has higher values in the sedimentary formation parallel to the bedding. Texture and mineralogical composition are instead the most significant variables. In addition, as indicated by Morales et al. [40], this type of material is heterogeneous by nature and is characterized by wide ranges of variation in its composition and in its physical, chemical and mechanical properties. Consequently, despite using the number of specimens stipulated in the standard test method, results would report significant dispersion associated with natural conditions of travertine formation. Hence, there will be no large difference in reported values by reducing the number of test specimens.

Durability assessment

To assess the durability of onyx-travertines, different accelerated aging tests were applied with the aim of determining their behavior under different environmental conditions, such as changes in temperature and exposure to freeze–thaw cycles, saline solutions and acids. These environmental conditions are commonly found in facades of buildings in the Historic Center of Cuenca.

F-T and T-S tests followed UNE-EN 12371 [41] and UNE-EN 14066 [42] standard test methods. The size of specimens and cycles for each test were adapted to the technical capacities available in the laboratory. Thus, the specimens employed were three 35 × 35 × 35 mm cubes of each type of travertine. For the F–T test, each cycle consisted of a freezing period of 16 h at a temperature of − 8 °C, followed by a thawing period of 8 h, in which the specimens were immersed in room temperature water. In the case of the laboratory, 20 ± 2 °C. The procedure lasted 80 cycles. In the thermal shock test, each cycle consisted of a heating period of 16 h at a temperature of 70 °C, followed by a cooling period of 8 h, in which the specimens were submerged in water at a temperature of 20 ± 2 °C for 80 cycles. The objective of these two tests was to determine the aging behavior of travertines under changes in temperature, given their use in facades of buildings in the Historic Center of Cuenca.

The S-C test was carried out according to a modified UNE-EN 12,370 [43] standard test method, where two 14% saline solutions were used: $Na_2SO_40.10H_2O$ and NaCl. Each cycle consisted of an 8 h immersion period of the specimens in the saline solution, followed by 16 h of drying in an oven (OSK 9500D Electric Oven) at 100 °C. The procedure lasted 50 cycles. Three specimens of each type of travertine were tested. The specimens were 35 × 35 × 35 mm cubes. NaCl solution was included in the test, since it is very common to find it on facades in the form of animal and human urine. $Na_2SO_4 \cdot 10H_2O$ was used to reproduce the damage caused by incompatible building materials in relation to onyx-travertine, such as cement in mortars [44].

The resistance due to the action of SO_2 test, followed the UNE-EN 13,919 [45] standard test method, with the same type of specimens described above and a 60% H_2SO_4 solution. This test was carried out to evaluate stone degradation due to aggressive environmental contaminants, such as the ones present in acid rain [46]. The test consisted of placing the specimens (previously immersed in water for 24 h) at 100 mm above the acid solution with the aid of a support, at a temperature of 20 °C for 21 days. At the end of the test, the specimens were washed with distilled water. Then, water absorption analysis was carried out. Three specimens were tested for each type of travertine. The specimens measured 35 × 35 × 35 mm.

Finally, the effect of accelerated aging tests (weather-related deterioration factors) was evaluated through visual examination and water-absorbed determination (in percentage) before and after each test by means of the analysis of variance (ANOVA) of a single factor. Calculation of the F factor was used as a measure of dispersion. Likewise, visual inspection and scanning electron microscopy were used to evaluate weathering

patterns in accord with the stone patterns weathering classification used in the field of conservation of Cultural Heritage [32].

Results and discussion

Mineralogical composition

Results of the mineralogical analysis of the onyx-travertines are shown in Table 1. XRD and SEM–EDS elemental analyses were combined for a holistic approach. It was determined that samples have calcite as the main component. Thus, GT is composed mainly of calcite. In PT, calcite has impurities such as hematite, manganite and siderite, providing its characteristic pink color. In WT, a mixture of calcite ($CaCO_3$) and relatively pure magnesite ($MgCO_3$) was found, showing a characteristic white color. Finally, YT is composed of a mixture of two polymorphs of calcium carbonate ($CaCO_3$), calcite and aragonite, with the presence of strontianite ($SrCO_3$), magnesite ($MgCO_3$) and hematite (in a lower concentration than in PT), yielding its yellow color. YT is of special interest because the test results have contributed to identifying the essential role played by strontianite in catalyzing the metastable nucleation of aragonite (precipitation of this carbonate polymorph from aqueous solution); since calcite is stable at low pressure and aragonite at a higher one. The backscattered electron micrograph and microchemical mapping (Fig. 4) show strontianite between two aragonite crystals, displaying the growth front of this polymorph and demonstrating that only in the presence of strontianite, does carbonate precipitate as aragonite. Otherwise, as proposed and discussed in previous studies, carbonate precipitates at that temperature and pressure only as calcite [47–49].

These results show how the presence of metal oxides or other colored minerals within the crystalline structure of onyx-travertine are the product of changes in precipitation and chemical composition of the spring, leading to the development of various colors [50–52]. This explains why onyx-travertine of different colors is found within the same mine.

Petrographic description

The four types of onyx-travertine studied show stratified sedimentary structures. PT and YT exhibit geometric characteristics consistent with porous laminated facies (typically 0.05 to 1 cm thick). In contrast, GT and WT present slightly porous cryptolaminated facies (millimetric layers) [53]. Specifically, YT has a microcrystalline texture (> 0.5 mm) [54], low roundness with a matrix dominated by hexagonal calcitic crystals perpendicular to pressure levels, and radioaxial and dendritic columnar crystals (Figs. 4c and 5b) with micrite, sparite and iron oxides cements with different structures: (a) acicular crystals in the form of spherules and fans (fibrous radiated) of Aragonite; (b) lamellar crystals of iron oxides forming microstromalites; (c) fragments of calcified canes or oncoids of considerable size (7–19 mm long and 0.15 mm wide) (Fig. 5a); (d) micrite peloids presumably of bacterial origin; and e) drusic sparite mosaic filling the pores.

PT exhibits a macrocrystalline texture (0.5–1 mm) [54] (Fig. 5d and e) with the presence of crystalline aggregates arranged in a mosaic configuration and dendrites of rhombic crystals (Fig. 5f) that suggests in situ competitive growth. It also has a laminated texture with alternating layers of laminar crystals of iron and manganese oxides/oxyhydroxides and layers of calcite meso- and/or macro-crystals (Fig. 5e). Aggregates of iron oxide crystals form wavy or contorted structures (microstromalites). The matrix is composed of carbonate crystals cemented by micrite, sparite and iron/manganese oxides.

GT has a microcrystalline texture, with acicular, dendritic columnar and radial crystals that are narrow at the base and widen towards the apical zone with a matrix of micrite and sparite (Fig. 5g). It includes cements of micrite, sparite and iron oxides with the following structures: (a) iron oxide crystals filling the space between calcite crystals (Fig. 5h), and (b) circumgranular acicular

Table 1 Mineralogical composition obtained by XRD

Test Specimen	Composition (%)							
	Calcite ($CaCO_3$)	Magnesite ($MgCO_3$)	Aragonite ($CaCO_3$)	Siderite ($FeCO_3$)	Strontianite ($SrCO_3$)	Anhydrite ($CaSO_4$)	Manganite (MnO(OH))	Iron oxide
PT	95.02	–	–	1.54	–	1.49	0.54	1.41
YT	65.50	9.69	23.91	–	< 0.5	< 0.5	–	< 0.5
GT	99.58	–	–	–	–	–	–	< 0.5
WT	76.57	22.57	–	–	–	0.86	–	–

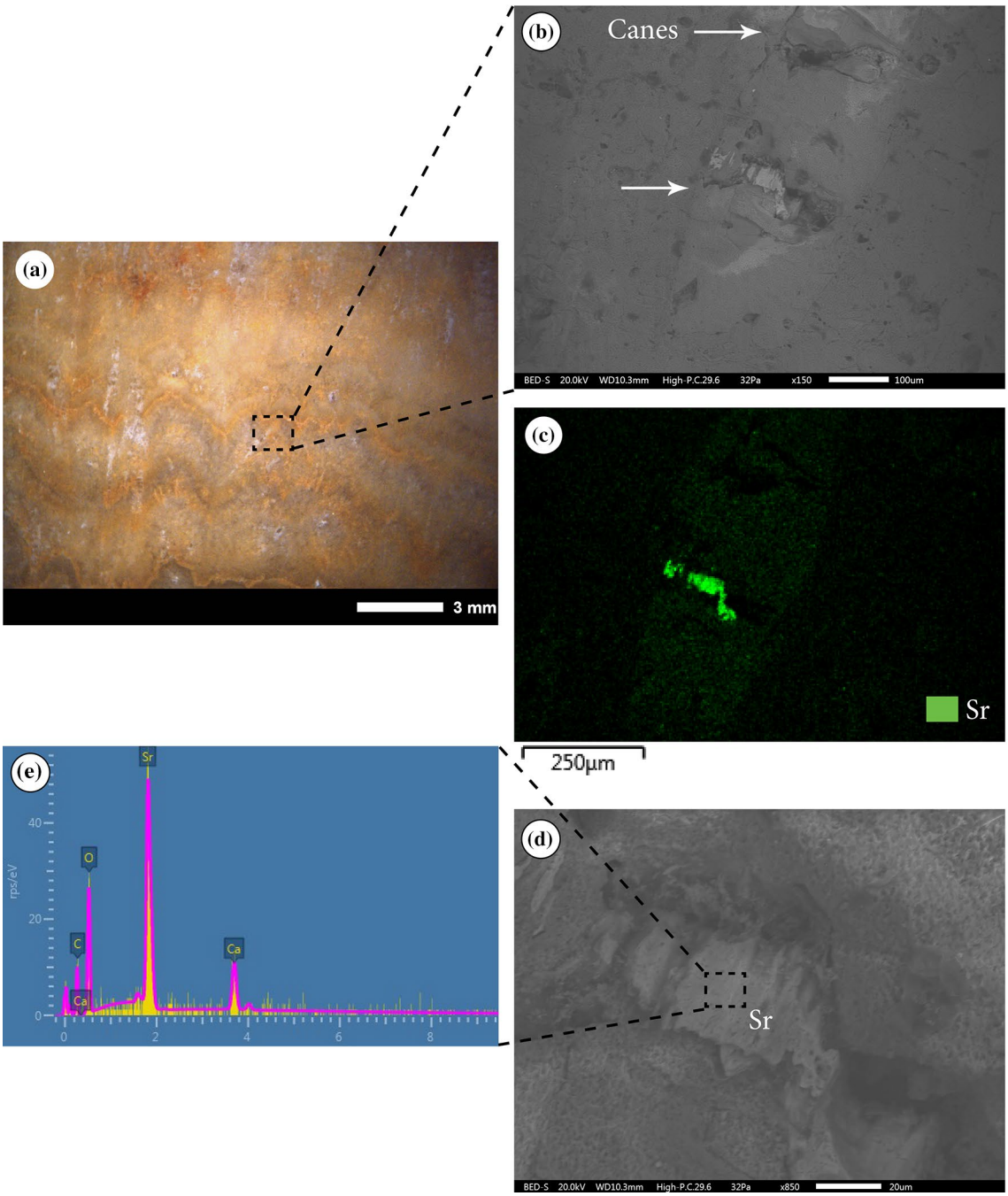

Fig. 4 **a** Optical micrograph of YT sample, **b** SEM micrograph of aragonite canes, **c** Microchemical mapping showing strontium in aragonite crystal of YT sample, **d** SEM micrograph of strontianite crystal, and **e** EDS spectrum of strontianite crystal

crystals. It also shows laminar bands of alternating layers of homogeneous elongated crystals and smaller crystals with a micritic matrix and iron oxides that give it a darker color (Fig. 5i).

WT exhibits a microcrystalline texture, low roundness with hexagonal crystals, radial acicular crystals and forming dendrites with micritic matrix (Fig. 5j and l). It also shows occluding carbonate cements with the following structures: (a) drusic sparite mosaic filling the pores; (b) small fragments of calcified or oncoid reeds (Fig. 5k); and (c) micrite peloids presumably of bacterial origin. Likewise, it presents angular clasts mainly of calcite

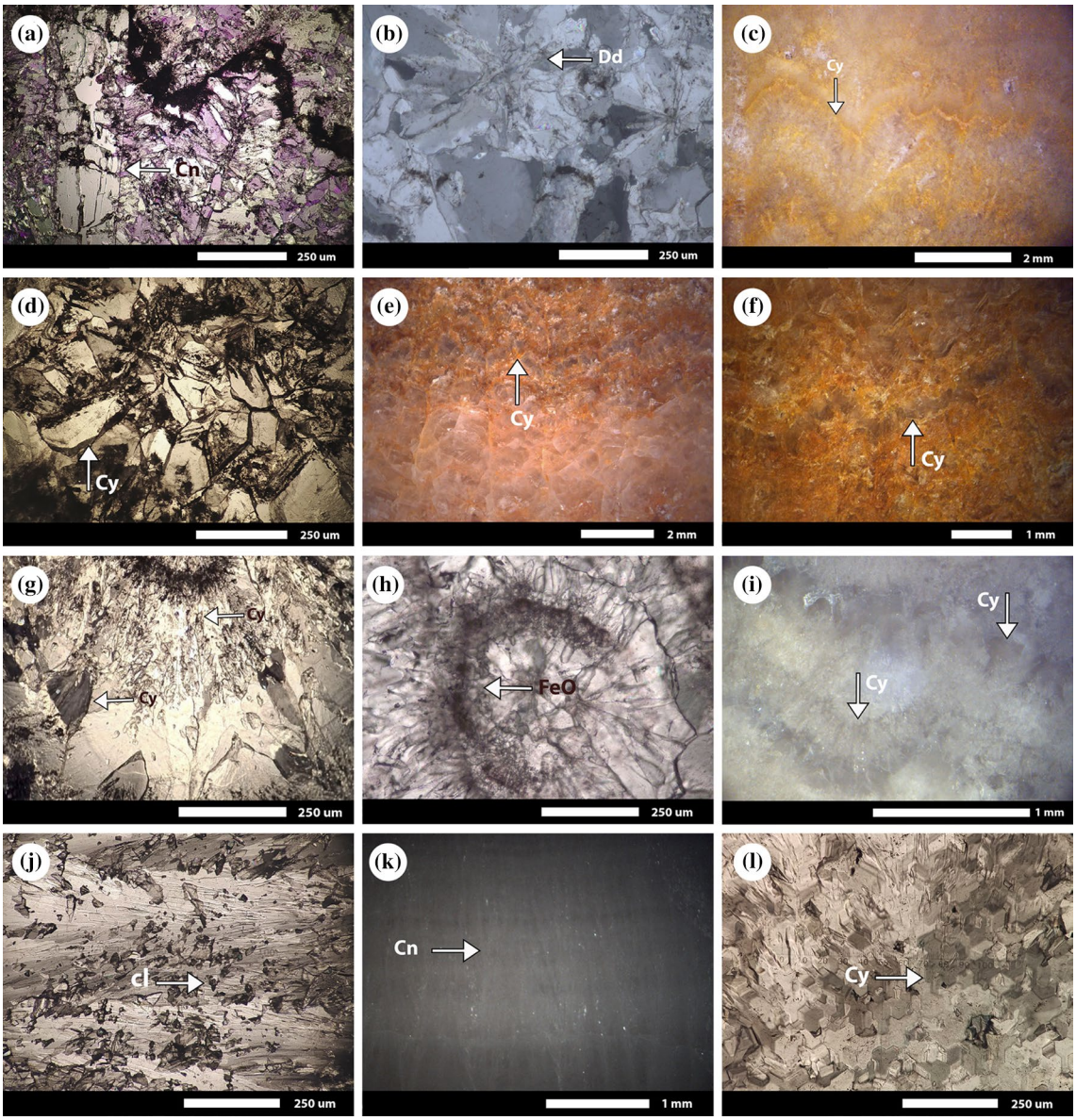

Fig. 5 Optical micrographs for petrographic analysis. In this figure, Cn stands for calcified canes, Dd stands for dendritic crystals, Cy stands for crystals, cl stands for clasts and FeO stands for Iron Oxide. **a** Columnar calcite crystals and calcified canes fragments in YT. **b** Dendritic crystals in YT. **c** Hexagonal crystals perpendicular to the laminated facies in YT. **d** Rhombic crystals with high roundness in PT. **e** Lamellar layers of iron oxides alternated with layers of iron oxyhydroxides in PT. **f** Dendrites of rhombic crystals in PT. **g** Crystals of different sizes between layers in GT, **h** Cements with iron oxides (red-brown color) covering calcite crystals in GT. **i** Elongated calcite crystals alternating with layers of small crystals on a micritic matrix in GT. **j** Undissolved angular clasts during stone formation in micritic matrix in WT. **k** Fragments of calcified reeds in YT. **l** Hexagonal crystals with low roundness in YT

(Fig. 5j) that were not able to dissolve in the hydrothermal fluid and were dragged during the formation of the stone.

Petrophysical description

Table 2 shows the results of real density, open porosity and water absorption, which are consistent with previously reported information. In general, onyx-travertine has a real density between 2.5 and 2.9 gr/cm^3, open porosity between 0.06 and 1.95% and water absorption between 0.01 and 0.05% [7, 55]. Furthermore, in Table 3 the statistical treatment presented shows significant differences between the studied onyx-travertine. Because, for all the parameters tested, the values of the

Table 2 Real density, open porosity and water absorption

Samples	Type of porosity		Real density (gr/cm^3)	Open porosity [%]	Capillary water absorption coefficient (gr/m^2 s$^{0.5}$)	Water absorption [%]
YT	Mesopores and macropores	μ	2.80	1.08	1.11	0.48
		σ	0.03	0.02	0.01	0.06
PT	Macropores	μ	2.53	0.68	0.69	0.17
		σ	0.03	0.05	0.02	0.06
GT	Mesopores	μ	2.70	0.52	0.55	0.08
		σ	0.03	0.05	0.01	0.02
WT	Mesopores and micropores	μ	2.61	0.26	0.41	0.03
		σ	0.04	0.03	0.03	0.01

Table 3 Analysis of variance of real density, open porosity and water absorption

	Origin of variations	Sum of squares	Degrees of freedom	Average of the squares	F	Probability	Critical value for F
Real density, (gr/cm^3)	Between groups	0.11	3	0.04	40.19	3.59E−05	4.07
	Within groups	7.20E^{-3}	8	9.00E^{-4}			
Water absorption [%]	Between groups	0.37	3	0.12	61.16	7.37E−06	
	Within groups	0.02	8	2.00E^{-3}			
Open porosity [%]	Between groups	1.07	3	0.36	223.89	4.70E−08	
	Within groups	1.27E^{-2}	8	1.60E^{-3}			
Capillary water absorption coefficient (gr/m^2 s$^{0.5}$)	Between groups	0.83	3	0.28	744.41	3.99E−10	
	Within groups	3.00E^{-3}	8	4.00E^{-4}			

experimental F test are greater than the critical F value, this confirms that these stones are very heterogeneous, as previously reported by other authors [30, 56]. On the other hand, according to the ASTM C1527/C1527M-1 [57] standard test method, the studied travertine samples meet the specifications for being used as architectural/construction material since they do not exceed 2.5% water absorption, therefore guaranteeing their quality.

Table 4 shows a summary of porosity classification for the studied travertines after Choquette and Pray [34]. In the laminated facies, there is greater diversity of non-fabric selective porosity produced during travertine diagenesis, which is mainly related to the deposition of iron oxides. In particular, YT has the highest values of porosity, with a predominance of mesopores (Fig. 6a) and macropores [34] in the lamellar facies. The effective porosity is mainly interparticle and fenestral, formed in the aragonite rod-type cements (Fig. 6b and c), which can reach millimeter size in length. The non-selective vugular porosity of different sizes and minimal interconnection with all the faces of the stone are located mainly in the calcified reeds. This is a product of the metastable nucleation of aragonite while precipitating in the presence of strontianite, and its further crystallization and cementation [58]. The effective porosity facilitates the transport of water to the interior of the stone, which is demonstrated by the higher values of absorption and capillarity.

PT has less porosity than YT. A predominance of macropores is identified in the laminated facies (Fig. 6d) formed by recrystallization and drusic mosaic-type cementation (Fig. 6f) that have partially covered the pores resulting from initial deposition and subsequent diagenesis. The open porosity is mainly interparticle selective and is located in the layers of iron oxides and oxyhydroxides formed during material deposition and in the cracks. To a lesser degree, non-selective vugular porosity (Fig. 6e) with sizes between 12 μm and 200 μm is present with interconnection.

Finally, WT and GT with cryptolaminated facies exhibited the lowest porosity values with the presence of sparitic cement filling the primary pores, generating a higher proportion of micropores (pores < 10 um) [34] than in the other travertines (Fig. 6i and l). Selective

Table 4 Type of porosity in specimens following classification by Choquette and Pray [34]

Samples	Cut direction	Porosity	
		Fabric selective	Non-fabric selective
GT	Parallel to lamination	Interparticle Intraparticle	Vuggy
	Normal to lamination	Interparticle	Vuggy Fenestral
YT	Parallel to lamination	Interparticle Intraparticle	Vuggy Fenestral
	Normal to lamination	Interparticle	Vuggy Fenestral
PT	Parallel to lamination	Intraparticle Interparticle	Vuggy Fracture Intercrystalline
	Normal to lamination	Intraparticle Interparticle	Vuggy Growth framework Fracture Intercrystalline
WT	Parallel to lamination	Interparticle	Vuggy
	Normal to lamination	–	Vuggy Fracture

fabric porosity of three types were identified to a lesser degree: interparticle, intraparticle, and fenestral (Fig. 6h and i). Also, to a lesser extent, irregular cavities that are more or less equidimensional and formed by non-selective dissolution were identified. Most of these porous structures have low interconnectivity.

Mechanical properties

For construction and decorative uses, compressive strength is a key property to be evaluated in building materials [59]. In Table 5, a summary of the mechanical strength obtained for the studied onyx-travertines is presented. In general, the strength of the parallel to lamination orientation has an average maximum strength of 99.75 MPa. Meanwhile, strength of the normal to lamination orientation is 64.41 MPa. This result demonstrates that the strength of the parallel to lamination orientation is 0.5 times greater than that of the normal to lamination orientation. Therefore, parallel to lamination orientation could be used for applications with vertical load-bearing capacity, such as facades; while normal to lamination orientation could be used for horizontal applications, such as flooring, without ignoring the architectural nature of the work [59] and the construction culture.

The greater strength of the parallel to lamination orientation is explained by pore distribution in the heterogeneous parallel bands. Pores are generally found in almost planar sections parallel to the stratification. Therefore, when loads are supported in the parallel to lamination orientation, the effective load-bearing area contains reduced porosity. In contrast, in the normal to the lamination orientation, the load-bearing area contains greater porosity sections leading to a lesser load-bearing resistance and failure of the element [53]. Consistently, travertines with cryptolaminated facies (less porous) show the best mechanical strength. This behavior has been reported previously by Akyol et al. [3].

In addition, the four types of onyx-travertine maintain constant values in maximum and minimum strength in the parallel to lamination orientation. After obtaining results from applying the UNE-EN 1926 [37] standard test method, the homogeneity and anisotropy typical of the variations in the porous system are clearly marked. In fact, a quasi- elastic behavior is observed at the parallel to lamination orientation and non-elastic behavior at the normal to lamination orientation, consistent with previously reported behavior of stones that are hydrothermally formed [60]. Consequently, the natural relationship between compressive and flexural strength and porous systems are also observed [59]. In the bending test, the obtained mean maximum strength in the parallel to lamination orientation is 9.66 MPa and in the normal to lamination orientation is 9.54 MPa. In any orientation, the strength is virtually the same. According to the values obtained for the four stones, the flexural strength is low, despite complying with the ASTM C 880-98 standard [61].

From these results, it can be seen that porosity is an important petrophysical characteristic, since it affects in a greater degree the stone's mechanical strength. For example, WT exhibits the best mechanical behavior by presenting the lowest porosity. Nevertheless, there are other parameters such as mineralogy that also influence this result in a lesser degree [62]. This can be shown by the fact that onyx-travertines finally demonstrate greater strength than would be expected if only porosity was taken into account.

Finally, in the compression and bending tests, the dispersion of results is high (Table 5). This coincides with other studies carried out worldwide for natural stones [3, 29, 59, 60], explained by their mineralogical characteristics and the difference in stratification and porous structures. Ultimately, these variations among travertines are expected and coincide with previous studies that show the same behavior.

From the results shown, it can be observed that onyx-travertines with higher thickness of layers in lamination/bedding also exhibit higher porosity values and lower

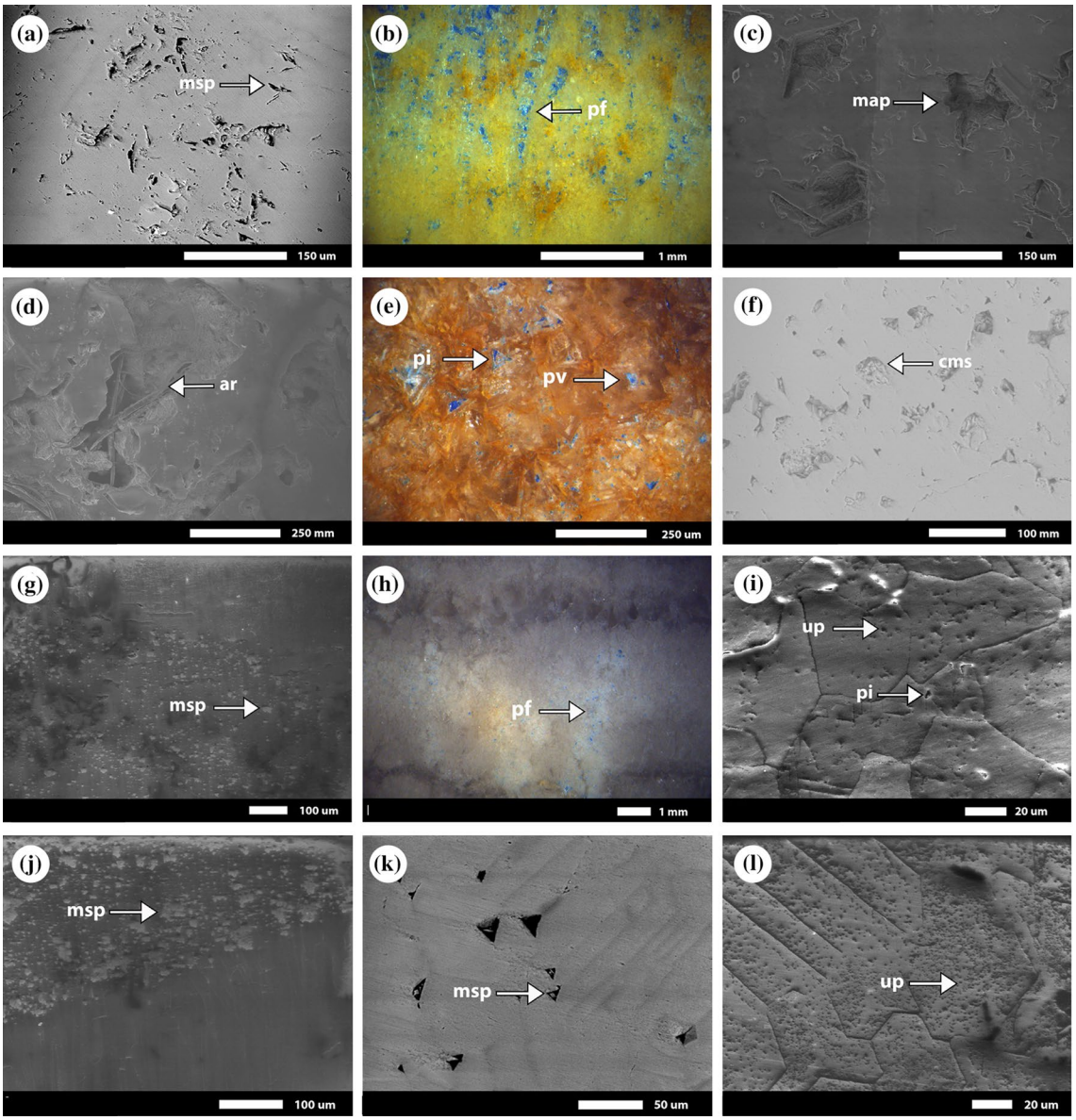

Fig. 6 In this figure, msp stands for mesopore, pf stands for fenestral porosity, map stands for macropore, ar stands for Aragonite, pi stands for intercrystalline pore, pv stands for vugular pore, cms stands for drusic mosaic cement, up stands for micropore. **a** SEM micrograph of Mesopores in YT. **b** Optical micrograph of fenestral porosity (in blue color) in YT. **c** SEM micrograph of macropores in calcified reeds in YT. **d** SEM micrograph of Aragonite filling macropores in PT. **e** Optical micrograph of vugular and intercrystalline porosity (in blue) in PT. **f** SEM micrograph of drusic mosaic cements filling the pores in a PT. **g** SEM micrograph of mesoporosity in bands with iron oxides in GT. **h** Optical micrograph of fenestral porosity perpendicular to precipitation facies in GT. **i** SEM micrograph of micropores and intercrystalline porosity in GT. **j** SEM micrograph of mesopores in calcified reeds in WT. **k** SEM micrograph of mesopores between calcite crystals in WT. **l** SEM micrograph of micropores between calcite crystals in WT

compressive strength, predominantly related to fenestral porosity. Authors attributed this behavior to its loss of layer packing density. Therefore, for the onyx-travertines studied, it is established that porosity is directly proportional to the thickness of layers (lamination/bedding) and compressive strength is inversely proportional to it.

Durability

The main objective of durability tests is to evaluate the effect of different environmental agents on the stones' degradation and to estimate their long-term resistance to salt crystallization, freezing–thawing, thermal shock and acid attack. Table 6 shows the dry weight loss

Table 5 Summary of mechanical strength

	YT	GT	PT	WT
Compression test				
Stone's strength in the parallel to lamination orientation				
Average strength (MPa)	91.83	96.88	93.03	117.26
Strength standard deviation (Mpa)	± 30.49	± 15.07	± 12.65	± 13.29
Strength variation coefficient	0.332	0.155	0.136	0.113
Stone's strength in the normal to lamination orientation				
Average strength (MPa)	79.61	83.17	51.09	43.78
Strength standard deviation (Mpa)	± 16.82	± 15.14	± 12.28	± 11.98
Strength variation coefficient	0.211	0.181	0.240	0.273
Bend test				
Stone's strength in the parallel to lamination orientation				
Average strength (MPa)	10.62	10.61	10.36	7.06
Strength standard deviation (Mpa)	± 5.50	± 1.02	± 1.21	± 5.62
Strength variation coefficient	0.518	0.096	0.116	0.795
Stone's strength in the normal to lamination orientation				
Average strength (MPa)	11.70	10.31	6.47	9.69
Strength standard deviation (Mpa)	± 6.01	± 57.59	± 2.03	± 2.34
Strength variation coefficient	0.513	1.527	0.261	0.200

(DWL) and water absorption (WA) before and after the accelerated aging tests. In addition, Table 7 presents the values of the F test (theoretical and calculated). From these results, it can be seen that stability of onyx-travertines against sudden changes in temperature, crystallization of salts, freeze–thaw and acid attack is different, not only in comparison with each individual analysis, but also when considering the two subtypes of onyx-travertines studied (laminated and cryptolaminated). These observations are consistent with the fact that the two subtypes are materials that have somewhat different physical characteristics, such as open porosity, type of pores and mechanical strength, as mentioned above.

On the other hand, the results presented in Tables 6 and 7 are consistent with other investigations [14, 16, 17, 19, 30, 63], which identify S-C and F–T as the deterioration mechanisms with the greatest impact on durability. As can be seen from the values of the F test (calculated from the experimental data), they turn out to have the highest negative impact in comparison to the other tests (S-C: YT = 207 and PT = 131). On the contrary, thermal shock shows lower values of calculated F test (YT = 23 and PT = 9), indicating little negative impact on the stone. In addition, a discussion of results of the accelerated aging tests follows.

Table 6 Water absorption [in percentage] before and after durability tests

Sample	Dry weight loss [%] (DWL)	Water absorption, WA [%] Before durability tests	Water absorption, WA [%] After durability tests
Freeze–Thaw (F–T)			
YT	− 0.53	0.48	0.72
PT	− 0.29	0.17	0.57
WT	− 0.07	0.03	0.05
GT	− 0.16	0.08	0.18
Thermal shock (T-S)			
YT	− 0.43	0.48	0.70
PT	− 0.31	0.17	0.33
WT	− 0.06	0.03	0.04
GT	− 0.15	0.08	0.14
NaCl crystallization			
YT	− 0.81	0.48	1.17
PT	− 0.70	0.17	0.67
WT	− 0.11	0.03	0.05
GT	− 0.40	0.08	0.19
Na_2SO_4 crystallization			
YT	− 0.85	0.48	1,14
PT	− 0.67	0.17	0.71
WT	− 0.17	0.03	0.06
GT	− 0.44	0.08	0.20
Acid Attack (A-A)			
YT	− 0.41	0.48	0.48
PT	− 0.30	0.17	0.17
WT	− 0.51	0.03	0.03
GT	− 0.42	0.08	0.08

The calculation of F was not performed for the acid attack tests. Water absorption [%] was the same before and after the test.

Salts crystallization (S-C)

Results show that laminated facies have higher DWL and WA values (F test) than the less porous cryptolaminated facies, demonstrating that there is a relationship between porosity and stone decay in salt crystallization, since porosity controls the ease of entry of saline solutions into the stones' porous network. Some researchers have reported that DWL has a positive correlation with effective porosity [30, 64, 65]; however, Akin and Özsan [14] found a negative correlation with effective porosity. The present study has demonstrated that the

Table 7 Analysis of variance for each durability test

Sample	Origin of variations	Sum of squares	Degrees of freedom	Average of the squares	Calculated F	Probability	Critical value for F tabulated
Freeze–Thaw (F–T)							
PT	Between groups	0.24	1	0.24	86.63	$7.00E^{-4}$	
	Within groups	0.01	4	$2.80E^{-3}$			7.71
YT	Between groups	0.09	1	0.08	22.48	$9.00E^{-3}$	
	within groups	0.02	4	$3.6\ E^{-3}$			
GT	Between groups	0.03	1	0.03	13.35	0.02	
	Within groups	0.01	4	$2.4E^{-3}$			
WT	Between groups	$4.00E^{-4}$	1	$4.00E^{-4}$	3.57	0.13	
	Within groups	$5.00E^{-4}$	4	$1.00E^{-4}$			
Thermal shock (T-S)							
YT	Between groups	0.07	1	0.07	22.96	$8.70E^{-3}$	
	Within groups	0.01	4	$3.10E^{-3}$			
PT	between Groups	0.04	1	0.04	9.04	0.04	
	Within groups	0.02	4	$4.30E^{-3}$			
GT	Between groups	$4.80E^{-3}$	1	$4.80E^{-3}$	3.28	0.14	
	Within groups	$5.90E^{-3}$	4	$1.15E^{-3}$			
WT	Between groups	$2.00E^{-4}$	1	$2.00E^{-3}$	1.50	0.29	
	Within groups	$4.00E^{-4}$	4	$1.00E^{-3}$			
NaCl crystallization							
YT	Between groups	0.70	1	0.70	207.02	$1.00E^{-4}$	
	Within groups	0.01	4	$3.40E^{-3}$			
PT	Between groups	0.37	1	0.37	131.37	$3.00E^{-4}$	
	Within groups	0.01	4	$2.80E^{-3}$			
GT	Between groups	0.02	1	0.02	16.79	0.02	
	Within groups	$4.10E^{-3}$	4	$1.00E^{-3}$			
WT	Between groups	$6.00E^{-4}$	1	$6.00E^{-4}$	6.00	0.07	
	Within groups	$4.00E^{-4}$	4	$1.00E^{-4}$			

relationship between these parameters is positive at 50 cycles for onyx-travertine.

In addition, $Na_2SO_4 \cdot 10H_2O$ turned out to be more aggressive that NaCl, which is attributed to its different hydration phases with different degrees of solubility [31, 66–68]. These hydration phases, after total or partial evaporation of the water, in their crystalline growth processes and in the transitions of the different hydration states, generate mechanical stresses that can deteriorate even the most compact and resistant stone materials [32, 69, 70]. Also, the rapid evaporation of water with temperature changes results in faster drying, leading to the appearance of subflorescences and thus higher crystallization pressures may occur [71]. This phenomenon was found by Celik and Ibrahimoglu in turkish travertines [17]. In contrast, the lower destructive potential of NaCl in laboratory tests has been attributed to its low tendency to supersaturation [21, 66] and its high tendency to form efflorescence rather than subflorescence [66, 72]. Therefore, it produces lower crystallization pressures within the pores.

SEM analyses identified similar weathering patterns in all samples that involve degradative processes that extended to all external surfaces as exfoliation, efflo-resces, granular desegregations, flaking or detachment. However, the intensity of weathering and its effect on the properties of onyx-travertines was higher in laminated onyx-travertines. Thus, in laminated travertines, an increase in the size of interparticle, intraparticle, vugular and fenestral pores was observed (Fig. 7a and b), especially in acicular crystals of the metastable phase Aragonite located in the reeds and in lamellar crystals of iron oxides in YT, and in layered calcite crystals with iron oxides present as microstromalites in PT. Disintegration of material was also recorded in vugular porosity, leaving larger voids completely empty. These weathering patterns are the result of mechanical stresses caused by salt crystal growth, which contributes to weight loss and

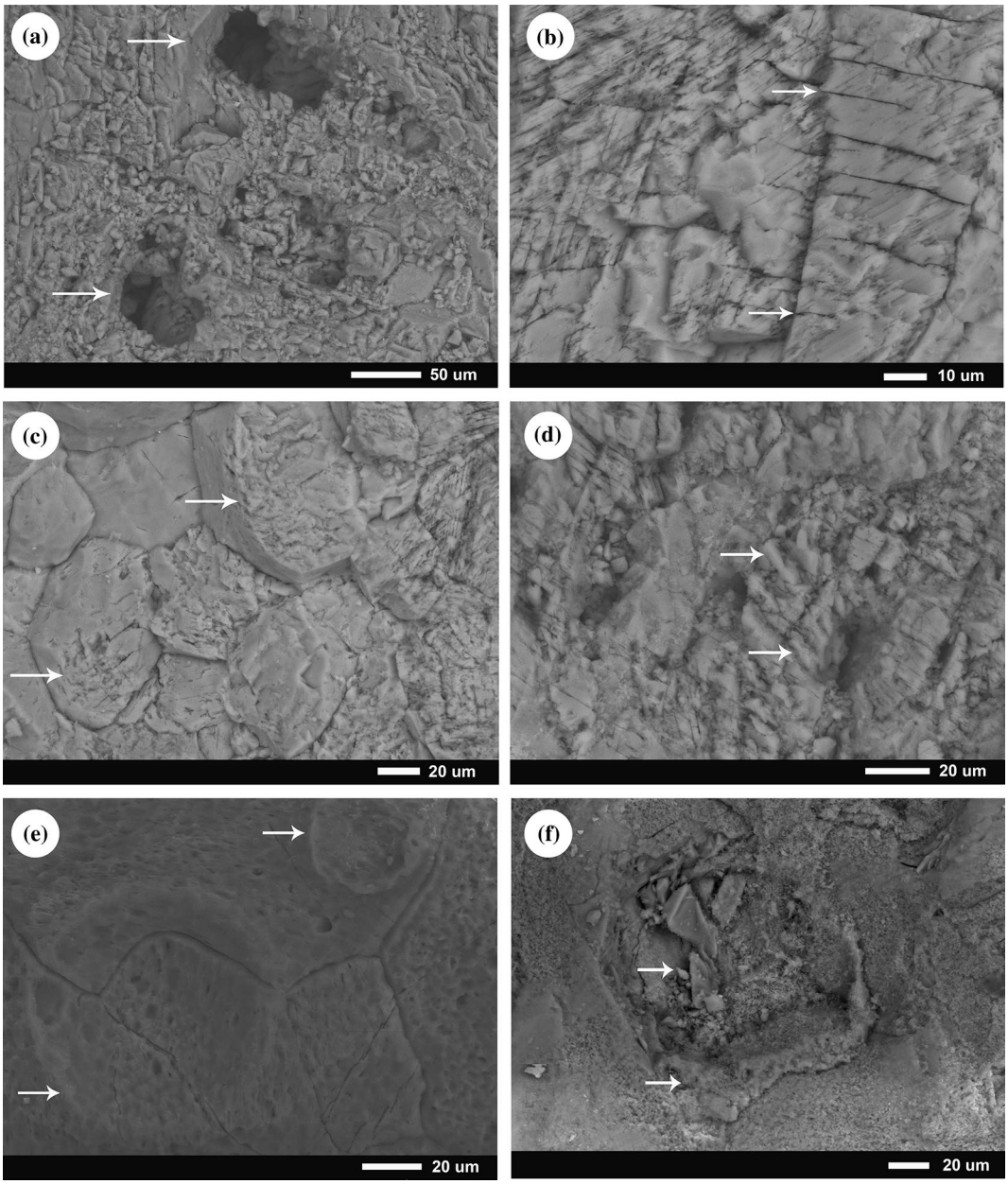

Fig. 7 Deterioration tests: **a** Increase in intraparticular porosity after salt crystallization test in PT, **b** Increase in porosity between hexagonal calcite crystals after salt crystallization in YT, **c** Exfoliation of crystals of calcite crystals after freeze–thaw test in GT, **d** Increase in intraparticular porosity in crystals fiber-radiated with iron oxides after freeze–thaw test in PT, **e** formation of cavities after the removal of gypsum crusts after acid attack test in WT and **f** dissolution of calcite crystals with the formation of gypsum after acid attack test in GT

increased pore size after testing and were also reported by Benavente et al. [15]. Some of the disintegrated material is redeposited on the surface as flakes or crusts.

Finally, the results show differences in DWL and WA values between laminated and cryptolaminated specimens because disintegration depends on some petrophysical factors such as effective porosity and pore type, since these parameters control the circulation of the solution in the stone. In the case of Sinincay onyx-travertine, DWL and WA increase with higher porosity and lower compressive strength; in particular, in the presence of fenestral porosity.

Freeze–thaw (F–T)

The DWL and WA values (F test) exhibit the same trend as the salt crystallization test: laminated onyx-travertines were more affected than the cryptolaminated ones. After water enters through the pores and temperature decreases, freezing occurs, expanding the water volume and causing an increase in the size and number of pores or microfractures, leading to an increase of the effective porosity. These weathering patterns were also recorded by means of Guler et al. [73].

The main weathering patterns are flakes or exfoliations visible to the naked eye in the normal to lamination orientation. In the SEM study, granular desegregation was observed starting in the pores and continuing through adjacent structures, generating an increase in pore size. Exfoliations of calcite crystals 1 to 5 µm thick were also recorded (Fig. 7c) as a result of the deleterious effect of these tests on the interparticle porosity of sedimentary structures containing iron oxides (generally hematite), which upon hydration, reduces the bonding forces between particles in the pore walls and thus acts as a plane of vulnerability under crystallization pressure (Fig. 7d). Finally, vugular pores were found to be empty due to granular decomposition and were observed not to be interconnected, thus not contributing further to increasing the effective porosity [74].

This work shows a direct relationship between effective porosity and WA, and an inverse relationship between these and the durability of onyx-travertine to F–T deterioration. As porosity increases, the stone's resistance to the pressure exerted by ice growth decreases. These relationships were previously reported by Zalooli et al. [75]. Their research showed that the effective porosity can be used to predict the UCS (uniaxial compressive strength), water absorption and durability of travertines with high reliability and degree of precision. It was also observed that, although the size of the vugular porosity can increase, it does not have a significant effect on the effective porosity because the interconnection is not taking place.

Acid attack (A-A)

After samples were subjected to acid corrosion, the formation of gypsum crystals ($CaSO_4 \cdot 2H_2O$) was observed on the faces exposed to the acid vapors due to calcite dissolution. As a result, the stone surface was chemically and physically eroded, causing some weathering patterns that resulted in weight loss. These results are consistent with those reported by other authors [27, 76].

In general, cryptolaminated onyx-travertines showed the strongest degradative processes and mass loss. SEM analysis showed WT as the most affected sample, with material detachments in the form of alveolar exfoliation between 70 and 250 µm in diameter and 10 µm deep (Fig. 7e). Condensation of H_2SO_4 occurs in the form of droplets on the surface of the stone, promoting subsequent reactions with $CaCO_3$, as the acid preferentially attacks the carbonate (CO_3) of the onyx-travertine in low pH acidic environments [76]. This pattern of decay has been recorded in past studies [29, 30]. It is important to point out that GT was less affected by this test, showing mainly an increase in roughness. By contrast, in the laminated onyx-travertines, the loss of material due to $CaSO_4$ crystallization was recorded inside the pores, promoting wall destruction and increasing pore size (Fig. 7f). Also, microfractures in the calcite crystals, especially in canes and in fenestral porosity, were established.

The results suggest that less porous cryptolaminated facies have more superficial $CaCO_3$ available to react with the acid vapors, so they are more affected by the dissolution of $CaCO_3$, which is distinctly shown by the alveolar exfoliation and loss of mass. It is also observed that this harmful effect is greater than that produced by the loss of material due to gypsum crystallization inside the pores.

Thermal shock (T-S)

The results of the T–S test were mainly manifested by color change in the onyx-travertine samples. They acquired a slightly yellowish tone and, at the same time, the DWL and WA values were the lowest in relation to the other tests. This may be explained by their calcareous nature, since there is little difference between shrinkage coefficients when exposed to different temperatures. In addition, a previous study has demonstrated that the porosity properties of marbles exposed to thermal effects do not affect the large or fine grains of calcite minerals [77], which are the main constituents of onyx-travertines.

Conclusions

The recognition of construction materials used in cultural heritage buildings through the characterization of their physical–mechanical properties and durability has defined a relevant framework for appropriate conservation interventions. However, it is evident that although there exist a variety of standards and recommendations according to the different variables or study objectives, there is still no universally agreed-upon methodology and, what is more serious, none of the methods provide criteria for classifying the durability of the tested material. This is the reality in Ecuador and in several parts of the world, which highlights the contribution of the present work, which makes use of standardized accelerated aging protocols and two quantitative parameters for the evaluation of deterioration, such as DWL and WA, as well as the morphometric recording of weathering

patterns by SEM images, in order to facilitate the intercomparison of the results of the different studies.

From the results of this study, it has been possible to determine that onyx- travertines of Sinincay (Cuenca) are stones composed primarily of calcite of hydrothermal and bacterial origin, characterized by the presence of stratification planes with different porosity that categorize them as porous laminated and poorly porous cryptolaminated, which, in turn, define their mechanical behavior and durability against natural and anthropic agents.

In general, after being subjected to aging tests, onyx-travertines showed an unweathered appearance at the mesoscale, but some of them experienced different types of weathering patterns with low intensity at the microscale. All samples showed surface granular disaggregation that contributed to weight loss and to the increased size of interparticle, intraparticle and fenestrated pores that resulted in an increased porosity and water absorption after durability tests. However, laminated facies suffered greater deleterious impact than cryptolaminated ones because the presence of iron oxides in the interparticle porosity and aragonite crystals in the fenestral porosity reduced the bond strength between pore walls and thus acted as a plane of weakness under ice and salt crystallization stresses. Thus, the inversely proportional relationship between porosity and deterioration resistance of onyx-travertine against these deterioration factors is demonstrated. Cryptolaminated facies suffered the greatest deterioration due to $CaCO_3$ dissolution when exposed to acid attack, generating alveolar exfoliation processes due to the greater effective superficial area available for the reaction.

From this investigation, it is concluded that the use of onyx-travertines as a construction and building material is appropriate. However, special attention must be paid to intrinsic factors such as the cut direction of the stone from extraction to preparation and the number of constituents (especially if abundant amounts of iron oxides are present) for defining its proper application. Other relevant factors that need to be taken into consideration for such purposes are: (1) the random placement of the stone in buildings with strong differences in anisotropy and properties; (2) the use of construction materials that can produce salts, such as cement or exposure to biological fluids that, like urine, are also salt producers; and (3) environmental factors, which have been impacted by climate change, with special emphasis on extremely low temperatures and pollution.

Furthermore, these findings also allow for the development of a different action framework for the conservation of these materials associated with architectural heritage, as well as its use in new buildings. Thus, given that the use of these onyx-travertines has defined the construction tradition of the city of Cuenca, as well as that of other cities around the world, it is important to promote their adequate and appropriate future use in order to maintain the iconic image of its historic urban landscapes.

In accordance with this new knowledge, it is necessary to pursue new perspectives and efforts in the particular determination of intervention strategies for the conservation and restoration of assets that use onyx-travertines. In addition, construction techniques with these materials will be improved by considering characteristics such as: porosity, mechanical strength, vulnerability to low temperatures, inappropriate use of non-compatible materials and environmental pollution in an articulated way. Finally, it is important to recognize that the current knowledge of historical building materials of Cuenca's Historic Center, and those of many other cities in Ecuador and Latin America, is limited and represents a multidisciplinary research niche with contributions that can have a great impact not only in the heritage field, but also in the construction demands of contemporary architecture and its role in promoting development.

Acknowledgements
The authors would like to thank the Universidad Católica de Cuenca (Ecuador) and the Instituto Nacional de Patrimonio Cultural (Ecuador) for providing analytical instruments and facilities for the development of this article and the research project in general.

Author contributions
Conceptualization: MRB, MCAU, MV. Contextualization: MCAU, JR. Methodology: MRB, MCAU, JR. Results and discussion: MRB, JR, MV, MCAU, EMCC. Conclusions: MRB, JR, MV, MCAU, EMCC. Writing and revision: MRB, JR, MV, MCAU, EMCC. Administrative management: MCAU, MRB. All authors read and approved the final manuscript.

Funding
This article is part of the research project No. PICVI19-09 called "Los materiales en el estudio histórico – constructivo—ambiental de los conjuntos históricos. El caso de Cuenca. ETAPA 2." belonging to the VI Institutional Call for Projects of the Universidad Católica de Cuenca (Ecuador). It has been developed under a specific inter-institutional cooperation agreement with the Instituto Nacional de Patrimonio Cultural. Also, the general methodological design for the study, data collection, laboratory tests, analysis, interpretation and writing has been carried out jointly by the technical teams of these institutions and the other coauthors.

Availability of data and materials
Datasets used and/or analyzed during the current study are available from the corresponding author on reasonable request. The Data and figures repository is found at https://drive.google.com/drive/folders/14RFrHhP3SBARbjMWKScRPXgLZF9Ei2tm.

Declarations

Competing interests
The authors declare that they have no competing interests. The funder had no role in the design of the study; in the collection, analyses, or interpretation of data; in the writing of the manuscript, or in the decision to publish the results.

Author details
[1]Research and Analysis Laboratory, Instituto Nacional de Patrimonio Cultural/National Institute of Cultural Heritage, Quito, Ecuador. [2]Universidad Politécnica de Madrid/Polytechnic University of Madrid, Madrid, Spain. [3]Universidad Católica de Cuenca/Catholic University of Cuenca, Americas Av, Cuenca 010101, Ecuador. [4]Universidad Internacional SEK/SEK International University, Quito, Ecuador.

Received: 4 July 2022 Accepted: 9 November 2022
Published online: 29 November 2022

References

1. Capezzuoli E, Gandin A, Pedley M. Decoding tufa and travertine (fresh water carbonates) in the sedimentary record: the state of the art. Sedimentology. 2014;61(1):1–21.
2. Ford TD, Pedley HM. Tufa deposits of the World. J Speleol Soc Jpn. 1992;17:46–63.
3. Akyol E, Yagiz S, Ozkul M, Sen G, Kato S. Physical properties of hot spring travertines related to lithotypes at Pamukkale region in Denizli, Turkey. In: Proceedings of First International Symposium on Travertine. 2005. p. 21–25.
4. Chafetz H, Folk R. Travertines; depositional morphology and the bacterially constructed constituents. J Sediment Res. 1984;54(1):289–316.
5. Guo L, Riding R. Hot-spring travertine facies and sequences, Late Pleistocene, Rapolano Terme, Italy. Sedimentology. 1998;45(1):163–80.
6. Yagiz S. Geomechanical properties of construction stones quarried in South-western Turkey. Sci Res Essays. 2010;5(8):750–7.
7. Marble Institute of America. Calcareous onyx. Tech Bull. 2011;6(1):1–12.
8. Calle MI, Espinoza PA. La Cité Cuencana: el afrancesamiento de Cuenca en la época republicana (1860–1940) [Trabajo de titulación de pregrado]. Cuenca: Universidad de Cuenca; 2002.
9. Sempértegui M, Vásquez M. De lo imaginario a lo consustancial. Colecciones memoria y patrimonio. In: Sempértegui M, editor. VV. AA. La ciudad de todas las orillas. Libro conmemorativo por el Bicentenario de la Independencia de Cuenca. Cuenca: Casa Editorial de Cuenca; 2020.
10. Aguirre Ullauri M del C. Materiales históricos, lectura histórico constructiva y caracterización. El caso de Cuenca (Ecuador) [Tesis Doctoral]. Madrid: Universidad Politécnica de Madrid; 2021.
11. Albornoz VM. Fundación de la ciudad de Cuenca en América: estudio histórico. The University of California; 1941.
12. Terán C. Índice Histórico de la Diócesis de Cuenca. Cuenca; 1919.
13. Wolf T. Geografía y Geología del Ecuador. Quito: Casa de la Cultura Ecuatoriana; 1892.
14. Akin M, Özsan A. Evaluation of the long-term durability of yellow travertine using accelerated weathering tests. Bull Eng Geol Environ. 2011;1(70):101–14.
15. Benavente D, Martinez-Martinez J, Cueto N, Ordoñez S, Garcia-del-Cura MA. Impact of salt and frost weathering on the physical and durability properties of travertines and carbonate tufas used as building material. Environ Earth Sci. 2018;77(4):147.
16. Cárdenes V, Mateos FJ, Fernández-Lorenzo S. Analysis of the correlations between freeze-thaw and salt crystallization tests. Environ Earth Sci. 2014;71(3):1123–34.
17. Çelik MY, İbrahimoglu A. Characterization of travertine stones from Turkey and assessment of their durability to salt crystallization. J Build Eng. 2021;43:102592.
18. Flatt RJ. Salt damage in porous materials: how high supersaturations are generated. J Cryst Growth. 2002;242:435–54.
19. Jamshidi A, Nikudel MR, Khamehchiyan M. Evaluation of the durability of Gerdoee travertine after freeze-thaw cycles in fresh water and sodium sulfate solution by decay function models. Eng Geol. 2016;202:36–43.
20. Yagiz S. The effect of pH of the testing liquid on the degradability of carbonate rocks. Geotech Geol Eng. 2018;36(4):2351–63.
21. Rodriguez-Navarro C, Doehne E. Salt weathering: influence of evaporation rate, supersaturation and crystallization pattern. Earth Surf Process Landf. 1999;24(3):191–209.
22. Ruiz-Agudo E, Rodriguez-Navarro C, Sebastián-Pardo E. Sodium sulfate crystallization in the presence of phosphonates: implications in ornamental stone conservation. Cryst Growth Des. 2006;6(7):1575–83.
23. Zehnder A. Salt weathering on monuments. In: First international symposium on the conservation of monuments in the Mediterranean basin. 1989. p. 31–58.
24. Rossi-Doria P. Laboratory tests on artistic stonework. In: Lazzarini P, editor. The deterioration and conservation of stone studies and documents on the cultural heritage. 16th ed. Paris: UNESCO; 1985. p. 235–42.
25. Bell FG. Durability of carbonate rock as building stone with comments on its preservation. Environ Geol. 1993;21(4):187–200.
26. Evans I. Salt crystallization and rock weathering: a review. Rev Géomorphologie Dyn XIX. 1970;153–177.
27. Parvizpour S, Jamshidi A, Sarikhani R, Ghassemi DA. The pH effect of sulfuric acid on the physico-mechanical properties of Atashkuh travertine, Central Iran. Environ Earth Sci. 2022;81(5):1–10.
28. Yagiz S. P-wave velocity test for assessment of geotechnical properties of some rock materials. Bull Mater Sci. 2011;34(4):947–53.
29. Jamshidi A, Nikudel MR, Khamehchiyan M, Zalooli A, Yeganehfar H. Estimating the mechanical properties of travertine building stones due to salt crystallization using multivariate regression analysis. J Sci Islam Repub Iran. 2017;28(3):231–41.
30. Zalooli A, Khamehchiyan M, Nikudel MR, Jamshidi A. Deterioration of travertine samples due to magnesium sulfate crystallization pressure: examples from Iran. Geotech Geol Eng. 2017;35(1):463–73.
31. Lubelli B, Cnudde V, Diaz-Goncalves T, Franzoni E, van Hees RPJ, Ioannou I, et al. Towards a more effective and reliable salt crystallization test for porous building materials: state of the art. Mater Struct Constr. 2018;51(55):1–21.
32. Positano M, Poli T, Toniolo L. Accelerated ageing by salt crystallisation: assessment of a suitable laboratory methodology. Heritage, Weather Conserv. 2006;575–81.
33. Dunham R. Classification of carbonate rocks according to depositional textures. Am Assoc Pet Geol Mem. 1962;108–121.
34. Choquette P, Pray L. Geologic nomenclature and classification of porosity in sedimentary carbonates. Am Assoc Pet Geol Bull. 1970;54:207–50.
35. Asociación Española de Normalización. UNE-EN 1936. Métodos de ensayo para piedra natural. Determinación de la densidad real y aparente y de la porosidad abierta y total. Madrid: Asociación Española de Normalización; 2007.
36. Asociación Española de Normalización. UNE-EN 1925. Métodos de ensayo para piedra natural. Determinación del coeficiente de absorción de agua por capilaridad. Madrid: Asociación Española de Normalización; 1999.
37. Asociación Española de Normalización. UNE-EN 1926. Métodos de ensayo para la piedra natural. Determinación de la resistencia a la compresión uniaxial. Madrid: Asociación Española de Normalización; 2007.
38. American Society for Testing and Materials. ASTM C99–87. Standard Test Method for Modulus of Rupture of Dimension Stone. West Conshohocken: American Society for Testing and Materials; 2000.
39. Ozkul M, Varol B, Alcicek M. Depositional environments and petrography of Denizli travertine. Bull Miner Res Explor. 2002;125:13–29.
40. Morales A, Azcaray M, Ordóñez M, Servín Martinez A, Hernández J. Caracterización físico-mecánica de dos travertinos de la región de Tepexi de Rodríguez, Puebla, México. In: Memorias del XXV Congreso internacional Anual de la SOMIM Materiales: Propiedad de los Materiales. Sinaloa; 2019.
41. Asociación Española de Normalización. UNE-EN 12371. Métodos de ensayo para piedra natural. Determinación de la resistencia a la heladicidad. Madrid: Asociación Española de Normalización; 2011.
42. Asociación Española de Normalización. UNE-EN 14066. Métodos de ensayo para piedra natural. Determinación de la resistencia al envejecimiento por choque térmico. Madrid: Asociación Española de Normalización; 2014.
43. Asociación Española de Normalización. UNE-EN 12370. Métodos de ensayo para piedra natural. Determinación de la resistencia a la cristalización de las sales. Madrid: Asociación Española de Normalización; 2020.
44. Romero M, Vásquez C, Espinoza F, Ramirez J. Caracterización de materiales de las fachadas del Centro Histórico de Cuenca y aproximación al diagnóstico de estado de conservación. Quito: Instituto Nacional de Patrimonio Cultural; 2021. 25-INPC-21.
45. Asociación Española de Normalización. UNE-EN 13919. Métodos de ensayo de piedra natural. Determinación de la resistencia al envejecimiento por la acción de SO2 en presencia de humedad. Madrid: Asociación Española de Normalización; 2003.

46. Haneef SJ, Johnson JB, Dickinson C, Thompson GE, Wood GC. Effect of dry deposition of NOx and SO2 gaseous pollutants on the degradation of calcareous building stones. Atmos Environ Part A Gen Top. 1992;26(16):2963–74.
47. Allison N, Finch AA, Sutton SR, Newville M. Strontium heterogeneity and speciation in coral aragonite: implications for the strontium paleothermometer. Geochim Cosmochim Acta. 2001;65(16):2669–76.
48. de Villiers S, Shen GT, Nelson BK. The SrCa-temperature relationship in coralline aragonite: Influence of variability in (SrCa) seawater and skeletal growth parameters. Geochim Cosmochim Acta. 1994;58(1):197–208.
49. Sunagawa I, Takahashi Y, Imai H. Strontium and aragonite-calcite precipitation. J Min Petrol Sci. 2007;102(3):174–81.
50. Ford TD, Pedley HM. A review of tufa and travertine deposits of the world. Earth Sci Rev. 1996;41(3–4):117–75.
51. Ranjbaran M, Zamanzadeh SM. Determining the role of chemical and biological factors in controlling precipitation of tufa and travertine deposits in Shurab area, Northern Iran. Carbonates Evaporites. 2021;36(4):1–18.
52. Reale R, Lovaglio T, Langerame F, Andreozzi G, Salvi AM, Sammartino MP. Spectroscopic investigation of iron stains on carbonatic stones. In: 6th international meeting on straightforward approach in cultural heritage and environment studies, multivariate analysis and chenometry; 2016 Dec 18–20; Roma, Italy. Roma: 2016. p. 5–6.
53. García-Del-Cura MÁ, Benavente D, Martínez-Martínez J, Cueto N. Sedimentary structures and physical properties of travertine and carbonate tufa building stone. Constr Build Mater. 2012;28(1):456–67.
54. Boggs S. Principles of sedimentology and stratigraphy. 5th ed. Boston: Prentice Hall; 2012.
55. Ersoy H, Yalçinalp B, Arslan M, Babacan AE, Çetiner G. Geological and geomechanical properties of the carbonate rocks at the eastern Black Sea Region (NE Turkey). J Afr Earth Sci. 2016;123:223–33.
56. Alves C, Figueiredo C, Maurício A, Braga MAS, Aires-Barros L. Limestones under salt decay tests: assessment of pore network-dependent durability predictors. Environ Earth Sci. 2011;63(7):1511–27.
57. American Society for Testing and Materials. ASTM C1527/C1527M-11. Standard Specification for Travertine Dimension Stone. West Conshohocken: American Society for Testing and Materials; 2018.
58. Dasgupta T, Mukherjee S. Porosity in carbonates. Adv Oil Gas Explor Prod. 2020. https://doi.org/10.1007/978-3-030-13442-6_2.
59. Çobanoğlu I, Çelik SB. Determination of strength parameters and quality assessment of Denizli travertines (SW Turkey). Eng Geol. 2012;129–130:38–47.
60. Goodman R. Introduction to rock mechanics. 2nd ed. Berkeley: Universidad de California; 1989.
61. American Society for Testing and Materials. ASTM C880/C880M-15. Standard Test Method for Flexural Strength of Dimension Stone. West Conshohocken: American Society for Testing and Materials; 2018.
62. Martínez-Martínez J, Benavente D, García del Cura MA. Petrographic quantification of brecciated rocks by image analysis. Application to the interpretation of elastic wave velocities. Eng Geol. 2007;90(1–2):41–54.
63. Zalooli A, Khamehchiyan M, Nikudel MR. Durability assessment of Gerdoi and red travertines from Azarshahr, East Azerbaijan province, Iran. Bull Eng Geol Environ. 2018;78(3):1683–95.
64. Benavente D, del Cura MAG, Fort R, Ordónez S. Durability estimation of porous building stones from pore structure and strength. Eng Geol. 2004;74(1–2):113–27.
65. Sousa LMO, Suárez del Río LM, Calleja L, Ruiz de Argandoña VG, Rodríguez Rey A. Influence of microfractures and porosity on the physico-mechanical properties and weathering of ornamental granites. Eng Geol. 2005;77(1–2):153–68.
66. Steiger M, Asmussen S. Crystallization of sodium sulfate phases in porous materials: the phase diagram Na_2SO_4–H_2O and the generation of stress. Geochim Cosmochim Acta. 2008;72(17):4291–306.
67. Rodriguez-Navarro C, Doehne E, Sebastian E. How does sodium sulfate crystallize? Implications for the decay and testing of building materials. Cem Concr Res. 2000;30(10):1527–34.
68. Desarnaud J, Bertrand F, Shahidzadeh-Bonn N. Impact of the kinetics of salt crystallization on stone damage during rewetting/drying and humidity cycling. J Appl Mech. 2013;80(2):0209111–7.
69. Juling H, Kirchner D, Brüggerhoff S, Linnow K, Steiger M, El Jarad A, et al. Salt damage of porous materials: a combined theoretical and experimental approach. In: 10th International Congress on Deterioration and Conservation of Stone. Stockholm; 2004. p. 187–94.
70. Hamilton A, Hall C. Mechanics of sodium sulphate crystal growth in the deterioration of sandstones: some new observations. In 10th International Congress on Deterioration and Conservation of Stone. Stockholm: Uniwersytet Śląski; 2004. p. 195.
71. Alves C, Vasconcelos G, Ferreira R. Salts in stone and mansory, advanced masters in structural analysis of monuments and historical constructions. In: Restoration and conservation materials. 2014. p. 2–50.
72. Diaz Gonçalves T. Salt crystallization in plastered or rendered walls. (Thesis PhD). Lisbon: Universidade Técnica de Lisboa; 2007.
73. Guler S, Türkmenoğlu ZF, Varol OO. Thermal shock and freeze-thaw resistance of different types of carbonate rocks. Int J Rock Mech Min Sci. 2021;137: 104545.
74. Jamshidi A, Nikudel MR, Khamehchiyan M, Zalooli A. Statistical models for predicting the mechanical properties of travertine building stones after freeze-thaw cycles. In: Lollino G, Giordan D, Marunteanu C, Christaras B, Yoshinori I, Margottini C, editors. Engineering geology for society and territory, vol. 8. Cham: Springer; 2015. p. 477–81.
75. Zalooli A, Khamehchiyan M, Nikudel MR. The quantification of total and effective porosities in travertines using PIA and saturation-buoyancy methods and the implication for strength and durability. Bull Eng Geol Environ. 2017;77(4):1739–51.
76. Singh TN, Sharma PK, Khandelwal M. Effect of pH on the physico-mechanical properties of marble. Bull Eng Geol Environ. 2006;66(1):81–7.
77. Vagnon F, Colombero C, Colombo F, Comina C, Ferrero AM, Mandrone G, et al. Effects of thermal treatment on physical and mechanical properties of Valdieri Marble – NW Italy. Int J Rock Mech Min Sci. 2019;116:75–86.

Publisher's Note